

# Interionic Interactions of Binary Gels Consisting of Pyrrolidinium-Based Zwitterionic Compounds and Lithium Salts

HoSeok Park,<sup>\*†</sup> Hoon Sik Kim,<sup>‡</sup> and Young Mee Jung<sup>§,\*</sup>

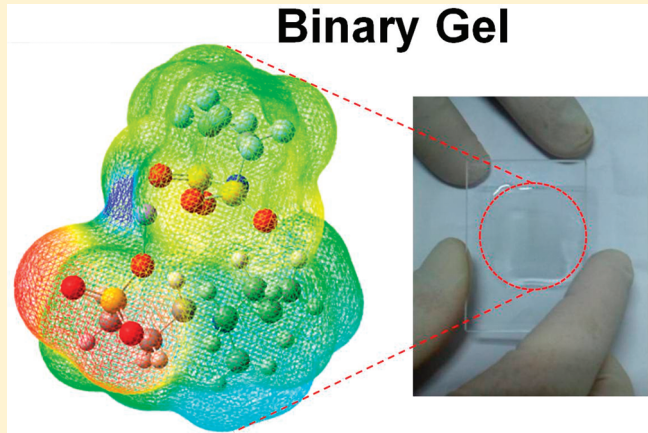
<sup>†</sup>Department of Chemical Engineering, College of Engineering, Kyung Hee University, 1 Seochon-dong, Giheung-gu, Yongin-si, Gyeonggi-do 446-701, Korea

<sup>‡</sup>Department of Chemistry and Research Institute of Basic Sciences, Kyung Hee University, 1 Hoegidong, Dondamoongu, Seoul, Korea

<sup>§</sup>Department of Chemistry and Institute for Molecular Science and Fusion Technology, Kangwon National University, Chunchon 200-701, Korea

 Supporting Information

**ABSTRACT:** We demonstrated thermal transitions and physical gelation of binary ionic salts through interionic interactions, which consist of pyrrolidinium-*N*-propanesulfonate zwitterionic compound (PyrZIC) and lithium bis(trifluorosulfonyl)imide (LiTFSI). The transition behaviors of binary ionic gels were attributed to conformational changes in the cations and anions of PyrZIC and LiTFSI as analyzed by density functional theory (DFT), principal component analysis (PCA), and two-dimensional infrared correlation spectroscopy (2D IR COS). Furthermore, the geometries of binary PyrZIC–LiTFSI systems were strongly influenced by the electrostatic interactions between two ionic salts. The different dynamic processes in the PyrZIC- and LiTFSI-rich phases, which are classified by the transition point of PCA plots, were induced by the conformational changes in the respective interaction fields, as shown by 2D correlation spectra. In particular, LiTFSI-rich binary gels revealed characteristic four-leaf-clover and butterfly patterns under their unique chemical circumstances, which were different from those of PyrZIC-rich gels. Consequently, these computational and experimental investigations provide an analytical tool to understand the physical phenomenon and interactions occurring in the unveiled and complicated systems.



## INTRODUCTION

The design and synthesis of ionic materials is a rapidly expanding area of material science for applications into electrolytes, acid–base chemistry, supramolecular assembly, confinement, enzymatic proton transfer, biological systems, drug delivery, and crystal engineering.<sup>1</sup> Intermolecular or interionic interactions are crucial to synthesizing ionic materials and invoking their emerging properties.<sup>1</sup> Ionic materials are associated with phenomena such as a facilitated ionic transport, a molecular recognition, and a thermal transition due to the complexity of secondary force fields.<sup>2</sup> The binary ionic gels described herein were readily synthesized through the neutralization of two ionic compounds or the formation of ionic liquid (IL)-like domains, exhibiting thermal transitions and physical gelation.

Recently, zwitter-type ionic compounds (ZICs), a new type of IL derivatives, have received much attention due to unique properties such as exceptional transport properties, efficient immobilization of carriers for molecular separation, and highly stable dispersion of nanoparticles.<sup>3</sup> ZICs can be used as precursors of binary ionic gels prepared through simple mixing with

ionic salts because of the intrinsic unique molecular structures,<sup>4</sup> which are composed of covalently tethered cations and anions.<sup>3</sup> Furthermore, ZICs were applied to lithium batteries due to their unique transport properties, such as increased conductivity and transference number of target ion.<sup>5</sup> Sun and Byrne et al. reported the enhancement of ionic conductivity of polyelectrolytes using ZICs as ion dissociators.<sup>6</sup> In particular, binary ionic gels including ZICs are extremely attractive because they require simple fabrication processes that mimic the synthesis of ILs, the so-called neutralization of two salts, and the emergent properties derived from the formation of coordinating molecular structure.<sup>7</sup> However, the mechanism of formation and dynamics of binary ionic gels have been thus far elusive.

The structures and interactions of ionic systems have been extensively investigated by a wide range of analytic methods such as UV–vis, IR, Raman, sum frequency generation (SFG), NMR, and X-ray spectroscopies.<sup>8</sup> For example, surface-sensitive vibra-

Received: July 6, 2010

Revised: November 25, 2010

Published: February 3, 2011

tional SFG spectroscopy has been used to study the effect of water on the surface of ILs.<sup>9</sup> However, these spectroscopic methods have difficulties in tracking conformational changes under specific environments and monitoring the dynamic process, due to overlapped peaks and restricted static information obtained from one-dimensional (1D) spectroscopy. Two popular and powerful spectroscopic techniques, principal component analysis (PCA) and two-dimensional infrared correlation spectroscopy (2D IR COS), can be used as analytical tools to unveil complicated interaction fields and dynamics. PCA provides a precise mathematical estimation of changes along sample and variable vectors.<sup>10</sup> 2D IR COS, which is generated by a cross-correlation analysis of dynamic fluctuations of IR signals induced by external perturbations such as temperature, time, stress, and concentration, is a well-established analytical technique to monitor the dynamic process of complex systems.<sup>11</sup> In addition, molecular geometries and energetic of ILs have been widely studied by density functional theory (DFT) in order to give theoretical evidence and support experimental results.<sup>12</sup> Izgorodina et al. demonstrated ion-pair binding energies of pyrrolidinium-based ionic liquids calculated by a range of DFT functionals.<sup>13</sup>

Here we report the synthesis and transitional behaviors of binary ionic gels consisting of pyrrolidinium-*N*-propanesulfonate ZIC (PyrZIC) and lithium bis(trifluorosulfonyl)imide (LiTFSI). Importantly, the analysis of binary ionic gels was theoretically and experimentally performed by DFT, 2D IR COS, and PCA. The computational and spectroscopic methods suggested herein are of prime importance for monitoring the dynamics in the multicomponent complex system as well as designing ionic materials with tailorabile properties.

## ■ EXPERIMENTAL SECTION

**Chemicals.** *N*-Methylpyrrolidine (97%) was purchased from Aldrich Co. 1,3-Propanesultone was a product of TCI Ltd. LiTFSI was supplied by Sigma Aldrich. Acetone (ACS agent) from Junsei Chemical Co. was distilled and stored with fresh 5 Å molecular sieves.

**Synthesis of Pyrrolidinium-*N*-propanesulfonate.** *N*-Methylpyrrolidine (100 mmol, 8.52 g) was mixed and stirred with 1,3-propanesultone (110 mmol, 13.4 g) in 100 mL of acetone for 24 h. The precipitated white solid product was collected by filtration. The product was washed with acetone and then dried under vacuum at room temperature. Yield: 96%.

<sup>1</sup>H NMR ( $D_2O$ , 300 MHz),  $\delta$  (ppm): 3.61 (t, 2H,  $CH_2$ ), 3.57 (m, 2H,  $CH_2$ ), 3.52 (t, 2H,  $CH_2$ ), 3.10 (s, 3H,  $CH_3$ ), 3.00 (t, 2H,  $CH_2$ ), 2.28 (t, 2H, Pyr), 2.24 (m, 4H,  $CH_2$ ).

Elemental analysis (%) for  $C_8H_{17}NO_3S$ : C, 47.10; H, 8.40; N, 6.87. Found: C, 47.14; H, 8.29, N, 6.85.

**Synthesis of Binary PyrZIC-LiTFSI (bi-PyrLi) Ionic Gels.** In order to fabricate bi-PyrLi ionic gels, PyrZIC and LiTFSI at the equivalent molar ratio were dissolved in a methanol solution. After the solution was stirred for 6 h, the resultant mixtures became transparent and colorless liquids. In order to remove methanol and impurities, the mixtures at the different molar ratios of PyrZIC and LiTFSI from 4:1 to 1:4 were dried in vacuum at 60 °C for 2 days. The resultant mixtures are denoted as bi-PyrLi 0–6 according to the molar ratio of PyrZIC and LiTFSI from 4 to 1 to 1 to 4, respectively. Homogeneous, transparent gel films were obtained by casting on a glass substrate.

**Density Functional Theory (DFT).** The interactions of PyrZIC with LiTFSI were examined through DFT calculations. The CPU time for each geometry is about 21 h and an altix 3700 system is used for calculation. Sixteen of 1300 MHz Itanium 2 CPU are installed in the system. To determine electronic wave functions, the DFT method was used with B3LYP (Becke's three-parameter hybrid exchange functional with the correlation functional of Lee, Yang, and Parr)<sup>14</sup>/6-311++G\*\* valence triple- $\zeta$  basis set.<sup>15</sup> The B3LYP is shown to accurately predict geometries and thermochemical data compared to generalized gradient approximation (GGA) and local density approximation (LDA). In addition, our energies included zero point energy corrections determined at the fully optimized structure with the same basis set. Geometries were regarded as optimized when the root-mean-square force, the root-mean-square displacement, the maximum force, and the maximum displacement of all atoms have values smaller than 0.00030, 0.00120, 0.00045, and 0.00180 amu, respectively. The binding energies of PyrZIC with LiTFSI in the optimized structures at standard state (298.15 K and 1 atm) were obtained from the following expression

$$E_b = E[\text{PyrZIC} + \text{LiTFSI}] - E[\text{PyrZIC}] - E[\text{LiTFSI}] \quad (1)$$

where  $E[\text{PyrZIC} + \text{LiTFSI}]$  is the enthalpy of the optimized structure of the PyrZIC–LiTFSI system at 298.15 K,  $E[\text{PyrZIC}]$  is the enthalpy of PyrZIC, and  $E[\text{LiTFSI}]$  is the enthalpy of LiTFSI. In the case of the self-association of LiTFSI, the binding energies in the optimized structures at standard state were obtained from the following expression

$$E_b = E[2 \times \text{LiTFSI}] - 2 \times E[\text{LiTFSI}] \quad (2)$$

where  $E[2 \times \text{LiTFSI}]$  is the enthalpy of optimized two LiTFSI system and  $E[\text{LiTFSI}]$  is the enthalpy of LiTFSI.

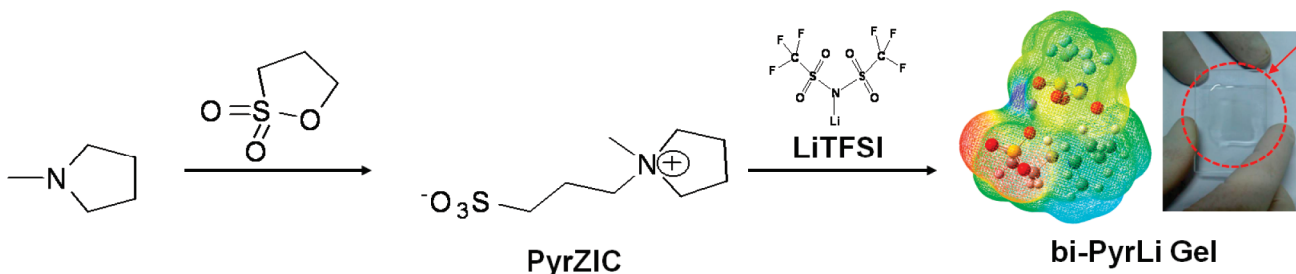
**Principal Component Analysis (PCA).** In PCA, the spectral data matrix ( $A$ ) is composed of the sum of an informationally significant portion  $A^*$  and a residual portion  $E$  comprising predominantly noise contributions. A significant portion decomposes the original spectral data matrix into a product of scores ( $W$ ) and loading ( $V$ ) matrices by PCA. Score matrix contains information on how samples are related to each other. The loading vectors represent the linear combinations of spectral contributions of actual components. The two matrices are linearly combined with the original data; hence in most discussions of PCA results, the two matrices are explored in parallel. The spectral data matrix ( $A$ ) can be expressed as the product of score ( $W$ ) and loading ( $V$ ) matrices by PCA.

$$A = A^* + E = WV' + E \quad (2a)$$

Here,  $V'$  stands for the transpose of  $V$ .

**Two-Dimensional IR Correlation Spectroscopy (2D IR COS).** In this study, 2D COS was applied to the concentration-dependent ATR spectra of bi-PyrLi ionic gel films prepared at the different molar ratios of PyrZIC and LiTFSI from 4:1 to 1:4. Generated by a cross-correlation analysis of dynamic fluctuations of IR signals induced by an external perturbation such as temperature, time, stress, concentration, etc., 2D IR COS is defined by two independent wavenumbers.<sup>16</sup> 2D IR COS is a well-established analytical technique that provides considerable utility and benefit for elucidating physical interactions such as intra- and intermolecular interactions and various spectroscopic studies of complex systems such as the formation mechanism of nanoparticles, biomaterialization, self/supramolecular assembly, dynamics of

**Scheme 1.** Illustration for the Synthesis Process of Binary PyrZIC-LiTFSI (bi-PyrLi) Ionic Gels by Simple Mixing of PyrZICs and LiTFSIs



ion or mass transport, and nanoconfinement.<sup>17</sup> Some of the notable features of generalized 2D correlation spectra are the following: simplification of complex spectra consisting of many overlapped peaks, enhancement of spectral resolution by spreading peaks along the second dimension, establishment of unambiguous assignments through the correlation of peaks of selectively coupled by various interaction mechanisms, and determination of the sequence of the spectral peak emergence.

The fundamental concept governing 2D correlation spectroscopy is a quantitative comparison of the patterns of spectral intensity variation along the external variable perturbation  $t$ , observed at two different spectral variables,  $\nu_1$  and  $\nu_2$ , over some finite observation interval. The 2D correlation spectra can be expressed as

$$X(\nu_1, \nu_2) = \Phi(\nu_1, \nu_2) + i\Psi(\nu_1, \nu_2) \quad (3)$$

$X(\nu_1, \nu_2)$  represents the quantitative measure of a comparative similarity or dissimilarity of spectral variations measured at two spectral variables,  $\nu_1$  and  $\nu_2$ . The intensity of a synchronous 2D correlation spectrum  $\Phi(\nu_1, \nu_2)$  represents the simultaneous or coincidental changes of two separated spectral intensity variations measured at  $\nu_1$  and  $\nu_2$ . The intensity of asynchronous 2D correlation  $\Psi(\nu_1, \nu_2)$ , on the other hand, represents sequential or successive, but not coincidental, changes of spectral intensities measured separately at  $\nu_1$  and  $\nu_2$ .

In a synchronous 2D spectrum, auto peaks located at the diagonal positions represent the overall susceptibility of the corresponding spectral region to change in spectral intensity as an external perturbation is applied to the system, while cross-peaks located at the off-diagonal positions of a synchronous 2D spectrum reveal simultaneous or coincidental changes of spectral intensities observed at two different spectral variables ( $\nu_1$  and  $\nu_2$ ). In contrast, an asynchronous 2D spectrum consisting of only cross-peaks provides useful information in order to interpret the mechanisms and kinetics of chemical/physical interactions: the relative temporal relationship or order of the actual sequence of reorientation processes.

**Characterization.** Differential scanning calorimetry (DSC, DuPont TA 2000), calibrated with indium, was used to monitor the changes of the thermal properties. All data were collected at a heating rate of 10 °C/min from -50 to 200 °C under N<sub>2</sub> atmosphere, after applying a heating cycle to remove water or other organic solvents: first run at a heating rate of 10 °C/min from 30 to 200 °C, following with a cooling step at a rate of 10 °C/min from 200 to -50 °C.

To analyze the thermal stability, thermogravimetric analysis (TGA) was carried out using a Dupont 2200 thermal analysis

station. Every sample was heated from 30 to 900 °C at a rate of 10 °C/min under an ambient air atmosphere.

ATR spectra were collected on a JASCO FT-IR 4100. The pressure was set as equal for all samples to avoid differences caused by the pressure and penetrating depth. Each spectrum, which was recorded as the average of 13 scans with a resolution of 4 cm<sup>-1</sup>, was collected from 4000 to 650 cm<sup>-1</sup>.

## RESULTS AND DISCUSSION

**Synthesis and Thermal Transitions of Binary Ionic Gel.** The bi-PyrLi ionic gels were prepared by simply mixing PyrZICs and LiTFSIs in a methanol solution as shown in Scheme 1. The resultant transparent and colorless mixtures were cast as homogeneous, transparent gel films on glass substrates. In order to evaluate the intrinsic properties of bi-PyrLi ionic gels, impurities were mostly removed by vacuum evaporation, as confirmed by DSC and TGA analyses. Given that both pristine PyrZIC and LiTFSI were solid powders at room temperature, the coordinating structures of two ionic compounds through the interionic interactions invoked changes in the physical properties of the mixtures and the formation of binary gels.

Thermal transitions of the PyrZIC–LiTFSI mixture were investigated via DSC and TGA analyses as shown in Figure 1. The DSC thermograms of pristine PyrZIC and LiTFSI and bi-PyrLi ionic gels revealed that the emergent fluidlike properties of the bi-PyrLi ionic gels are related to having  $T_g$  below room temperature. The  $T_g$  of PyrZIC and LiTFSI was not detected below room temperature. Furthermore, two sharp endothermic peaks attributed to  $T_m$  of LiTFSI at 317.0 and 424.6 K completely disappeared after mixing PyrZIC with LiTFSI. Pristine PyrZIC was in a solid, powdery state due to its intrinsic structure of covalently tethered cations and anions and strong interionic interactions. Meanwhile, LiTFSI showed no glass transition behavior because of the restriction of rotation by the interactions between lithium ions and TFSI anions. The breakdown of inherent crystalline structures of two salts in the compositional range evaluated in this study, which was largely associated with the coordinating structures of the bi-PyrLi ionic gels, resulted in no endothermic peak attributable to melting temperature near room temperature and the formation of ionic gel. The existence of respective crystalline structures of binary gels indicates that their unique thermal transition behaviors were related to a structural arrangement of two components (see Figure S1). These results were attributed to the coordinating function of PyrZIC, which leads to the weakening and even breaking of the ionic bonds between each LiTFSI ion by perturbing the existing force fields.<sup>18</sup> In a similar manner to the formation of ILs by

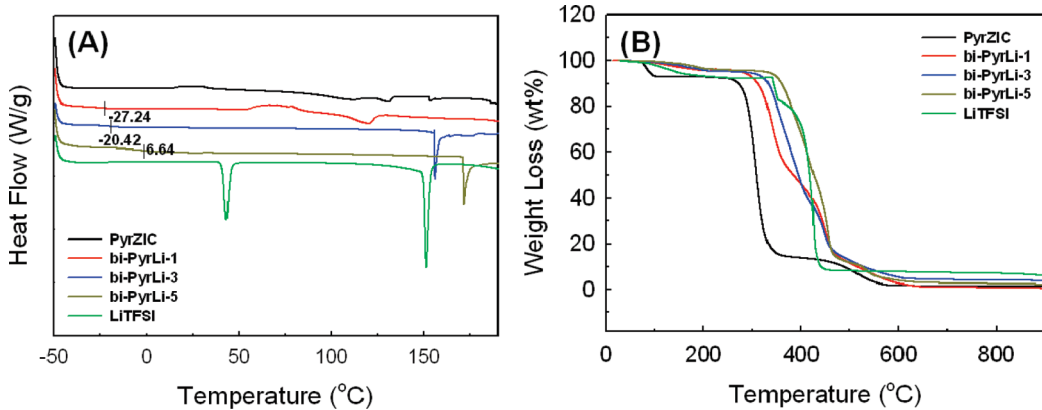


Figure 1. (A) DSC and (B) TGA curves of PyrZIC, LiTFSI, and bi-PyrLis.

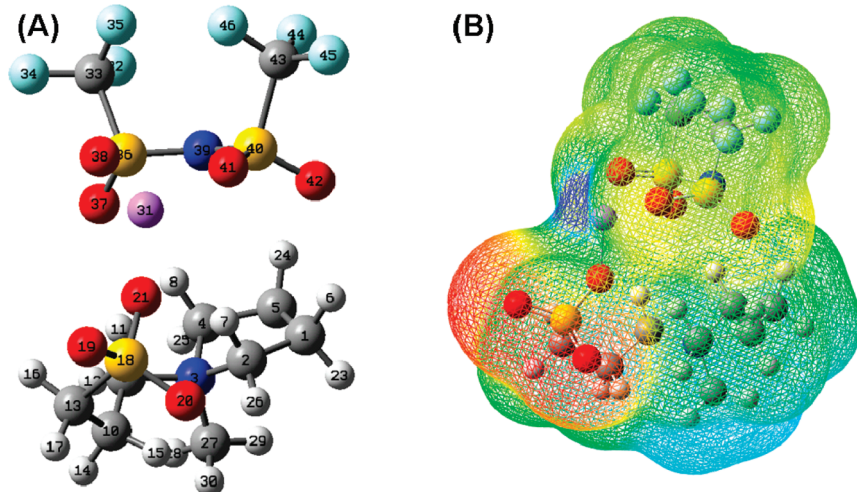


Figure 2. (A) Optimized geometries and (B) surface charge density for PyrZIC–LiTFSI (see Tables S1 and S2, Supporting Information, for the notation of individual atoms).

neutralization of two ionic salts,<sup>7</sup> the specific interactions between the pyrrolidinium rings of PyrZICs and TFSI anions of LiTFSIs and antisymmetric structures of the binary gels reduced the lattice energies and enhance mobility,<sup>19</sup> thereby triggering the emergence of  $T_g$ . Furthermore, the formation of binary IL-like domains in the bi-PyrLi ionic gels disrupts individual molecular packing and hinders crystallization into a solid phase, inducing the disappearance of  $T_m$  of the LiTFSI. In contrast, the bi-PyrLi ionic gels improved the thermal stability of PyrZIC from  $\sim 640$  to  $\sim 710$  K in accordance to the concentration of LiTFSI, in a tendency similar to that of previous studies.<sup>20</sup> The unique changes in thermal transition and degradation could be rationalized by the interactions between PyrZIC and LiTFSI via electrostatic interactions and the formation of binary IL-like domains. Therefore, the interionic interactions of the binary ionic gels should be theoretically and experimentally analyzed on the basis of the reflection of the changes in the thermal transition.

**Analysis of the Interactions of Binary Ionic Gel by DFT.** The interactions between PyrZICs and LiTFSIs at the molecular level were theoretically analyzed by DFT. The geometries of PyrZIC interacting with LiTFSI in the optimized structure at the standard state were obtained from 6-311+G\*\*, as shown

in Figure 2. The geometries of PyrZIC–LiTFSI in the optimized state also provide details of the bond distances, bond angles, and dihedral angles of the systems (see Table S1). In the optimized geometries of PyrZIC–LiTFSI, hydrogen atoms of PyrZIC interact with oxygen atoms of the TFSI group ( $d = 2.27$  Å for 8–36 and  $d = 2.32$  Å for 10–26). The lithium cation of LiTFSI interacts with an oxygen atom bound to a sulfonate group of PyrZIC via electrostatic interactions ( $d = 2.05$  Å for 41–23 and  $d = 1.97$  Å for 41–25). Since the binding energies of geometries of PyrZIC–LiTFSI ( $E_b = -42.1$  kcal/mol) are greater than the self-association energy of LiTFSI ( $E_b = -29.78$  kcal/mol) (see Table S2), LiTFSI molecules can be dissociated into lithium and sulfonate ions or solvated by interaction with PyrZICs. The interionic interactions between lithium ions and sulfonate groups or TFSI anions and pyrrolidinium rings induce the energetic stabilization of binary ionic gel by the charge delocalization of PyrZIC–LiTFSI. TFSI anion interacts with the pyrrolidinium ring as an acidic part of PyrZIC (electronic charge deficiency, indicated in blue in Figure 2b) via hydrogen bonding, while the lithium cation interacts with sulfonate groups as a basic part of PyrZIC (electronic charge sufficiency, indicated in red in Figure 2b) via electrostatic interactions. The electrostatic potential on an isosurface of electronic density

around PyrZIC—LiTFSI reaches equilibrium through the minimization of free energy.

**Analysis of the Interactions of Binary Ionic Gel by PCA and 2D IR COS.** For a deep understanding of the dynamics of the thermal transitions and physical gelation in the binary ionic gels, concentration-dependent IR spectra of the bi-PyrLi ionic gels were obtained, as shown in Figure 3. The representative bands regarding the pyrrolidinium rings and sulfonate groups of PyrZICs and the TFSI anions of LiTFSIs in the range  $1400\text{--}1000\text{ cm}^{-1}$  were particularly focused in the context of the formation of coordinating structures. For the IR spectra of PyrZICs, the in-plane C—H and twisting C—H of the pyrrolidinium rings and  $\nu_a\text{S=O}$  of sulfonate groups were assigned to  $1175$ ,  $1130$ , and  $1050\text{ cm}^{-1}$ , respectively. For the IR spectra of LiTFSIs, in-phase  $\nu_s\text{S=O}$ ,  $\nu_a\text{S=O}$ , and out-phase  $\nu_s\text{S=O}$  were assigned around  $1350$ ,  $1320$ , and  $1190\text{ cm}^{-1}$ , respectively. Considering that the bands related to the pyrrolidinium rings, sulfonate, and TFSI groups in bi-PyrLi system shifted and

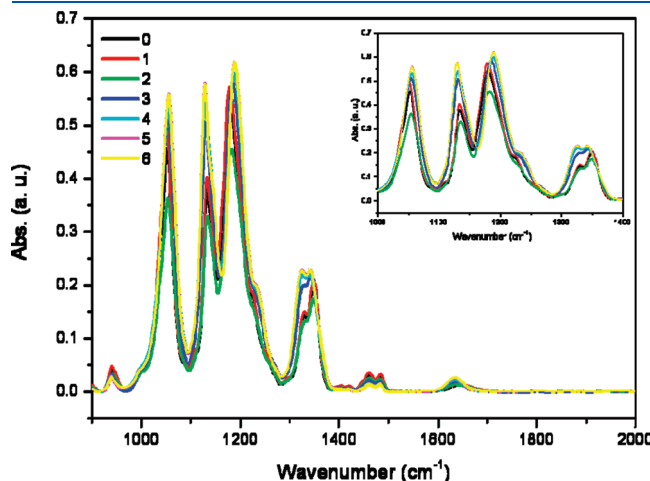
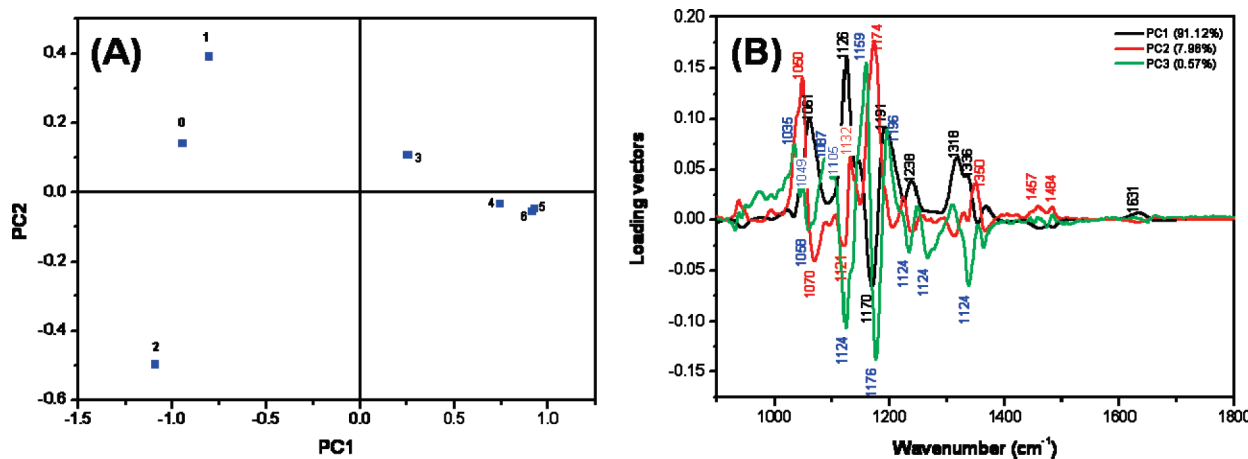


**Figure 3.** FT-IR spectra of bi-PyrLis as a function of chemical compositions in the range  $2000\text{--}900\text{ cm}^{-1}$ . The numbers 0, 1, 2, 3, 4, 5, and 6 mean a molar ratio of PyrZIC and LiTFSI of 4 to 1, of 3 to 1, of 2 to 1, of 1 to 1, of 1 to 2, of 1 to 3, and of 1 to 4, respectively. Inset is an enlarged image of FT-IR in the range  $1400\text{--}1000\text{ cm}^{-1}$ .

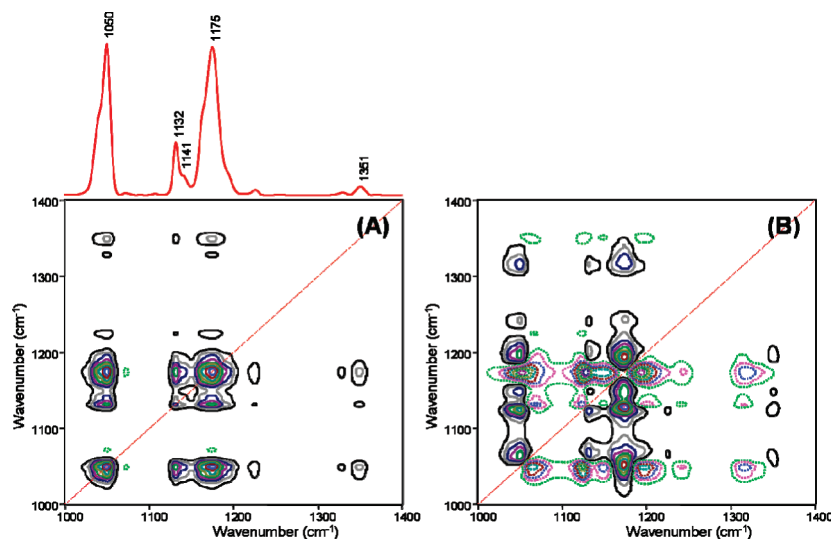
weakened compared to that of the pristine PyrZIC, however, it was confirmed that the conformational changes occurred via the electrostatic interactions. This finding is supported by the fact that the characteristic bands of the pyrrolidinium rings in UV-vis spectra of PyrZICs were blue-shifted and weakened with the increase in the concentration of LiTFSIs (see Figure S2).

Figure 4 shows PCA scores and loading plots derived from the concentration-dependent FT-IR spectra to capture the transition behaviors according to the chemical compositions. The score values of PC1 and PC2 clearly deconvoluted FT-IR spectra into two regions I and II. The PC1 contributes to 91.12% of the overall change in the spectra, whereas the PC2 and PC3 only capture 7.96% and 0.57% of the remaining variances not described by PC1. The bi-PyrLi ionic gels exhibited an apparent turnover of PC1 from negative to positive values at a molar ratio of 1 to 1. This turnover point from region I to region II captured by PCA was related to the changes in the thermal properties and the structural rearrangement. Furthermore, the ionic transport of binary ionic gels changed with respect to chemical composition, as previously reported.<sup>4</sup> The first PC is indicative of physical phenomena related to the greatest amount of variation in the data.<sup>10</sup> Consequently, the observation of highly positive PC1 loadings at  $1318$ ,  $1191$ ,  $1126$ , and  $1061\text{ cm}^{-1}$  elucidates that the thermal transition and physical gelation of binary ionic gels were induced by the conformational changes in the pyrrolidinium rings and sulfonate groups of PyrZICs and TFSI anions of LiTFSIs, accompanied by the different dynamic processes in the regions I and II.

2D IR COS was used to analyze the respective dynamic behaviors of regions I and II, which were divided by PCA. Figures 5 and 6 show synchronous and asynchronous 2D correlation spectra of regions I and II, respectively. In a synchronous 2D correlation spectrum, the strong auto peaks located on the main diagonal represent the overall susceptibility of the corresponding spectral region to change in spectral intensity as an external perturbation is applied to the system.<sup>11</sup> The synchronous 2D correlation spectrum for region I revealed dramatic changes of peaks at  $1175$  and  $1050\text{ cm}^{-1}$ , while that for region II exhibited dominant peaks at  $1197$ ,  $1174$ , and  $1126\text{ cm}^{-1}$ . Obviously, the former showed the depression of two characteristic



**Figure 4.** (A) Scores and (B) loading vectors of PC1 (91.12%), PC2 (7.96%), and PC3 (0.57%) for the concentration-dependent FT-IR spectra of bi-PyrLis. The numbers 0, 1, 2, 3, 4, 5, and 6 mean a molar ratio of PyrZIC and LiTFSI of 4 to 1, of 3 to 1, of 2 to 1, of 1 to 1, of 1 to 2, of 1 to 3, and of 1 to 4, respectively.



**Figure 5.** (A) Synchronous and (B) asynchronous 2D correlation spectra of the PyrZIC-rich phase (region I) in the range 1000–1400 cm<sup>-1</sup>. Solid and dashed lines represent positive and negative cross-peaks, respectively.

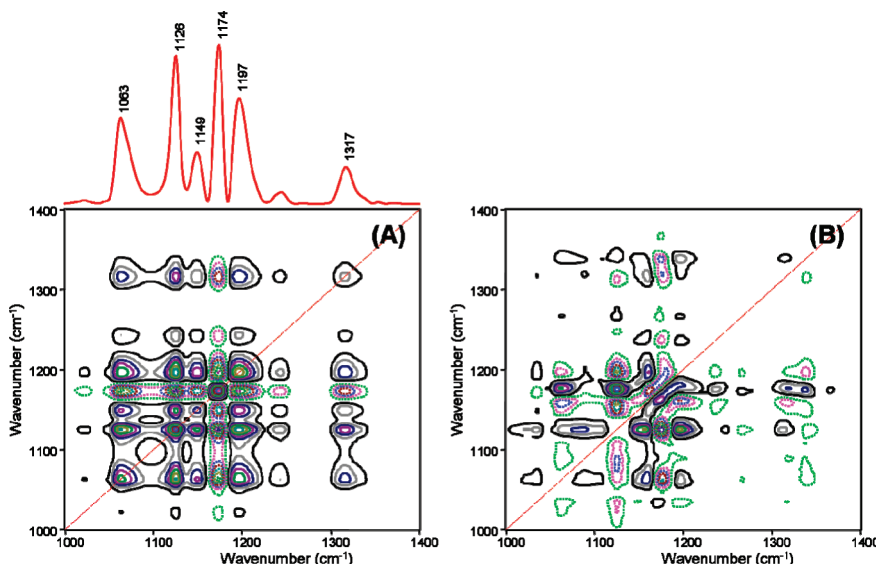


**Figure 6.** (A) Synchronous and (B) asynchronous 2D correlation spectra of the LiTFSI-rich phase (region II) in the range 1000–1400 cm<sup>-1</sup>. Solid and dashed lines represent positive and negative cross-peaks, respectively.

peaks at 1317 and 1197 cm<sup>-1</sup>, and the shift of the peak position due to the unique dynamic behaviors differing from the latter. The synchronous 2D correlation spectrum for region II shows the characteristic pattern of a four-leaf-clover cluster, consisting of two auto peaks at 1197 and 1174 cm<sup>-1</sup> and two negative cross-peaks. Moreover, the corresponding asynchronous 2D correlation spectrum apparently reveals a characteristic butterfly pattern for the peak position shift due to the conformational changes under the different chemical circumstances. Given that a synchronous 2D correlation spectrum exhibits simultaneous changes in spectral intensities that are observed at two spectral variables ( $\nu_1$  and  $\nu_2$ ), the interrelation of conformational changes attributable to the intermolecular interactions can be interpreted by the cross-peaks located at the off-diagonal positions.<sup>11</sup> The positive cross-peaks at (1351, 1175), (1132, 1175), and (1050, 1175) cm<sup>-1</sup> in the synchronous 2D correlation spectrum in

region I demonstrate that the variation of spectral intensity of a peak at 1175 cm<sup>-1</sup> was strongly interrelated with those at 1351, 1132, and 1050 cm<sup>-1</sup>. It means that the conformational changes of the pyrrolidinium rings were derived from those of the TFSI anions of LiTFSIs and/or the sulfonate groups of PyrZICs through interionic interactions. In the case of region II, one peak near 1197 cm<sup>-1</sup> revealed positive interrelation among conformations identical to region I, while the other peak at 1174 cm<sup>-1</sup> exhibited reciprocal behavior of simultaneous spectra variation. It is worthwhile noting that the additional peak captured in region II leads to thermal transitions and physical gelation because of the unique dynamic behavior, which results in more complex interaction fields compared to region I.

An asynchronous 2D correlation spectrum, which consists only of cross-peaks, is useful to analyze the kinetics of the chemical/physical reactions because of the relative temporal

relationship and actual sequence of individual reaction processes.<sup>11</sup> For the demonstration of the different dynamic behaviors of the two regions I and II, the respective kinetics of the conformational changes were studied by asynchronous 2D correlation spectra. Analysis of 2D correlation spectra in the two regions shows the following sequence of changes in spectral intensities by resolving overlapped peaks: 1174 (in-plane C—H, pyrrolidium ring of PyrZIC) → 1351 (in-phase  $\nu_s S=O$ , TFSI anion of LiTFSI) → 1050 ( $\nu_a S=O$ , sulfonate group of PyrZIC) → 1134 (twisting C—H, pyrrolidium ring of PyrZIC) → 1193 (out-phase  $\nu_s S=O$ , TFSI anion of LiTFSI) → 1151 (twisting C—H, pyrrolidium ring of PyrZIC) → 1122 (twisting C—H, pyrrolidium ring of PyrZIC) → 1314 ( $\nu_a S=O$ , TFSI anion of LiTFSI) → 1064 ( $\nu_a S=O$ , sulfonate group of PyrZIC)  $\text{cm}^{-1}$  in region I and 1156 (twisting C—H, pyrrolidium ring of PyrZIC) → 1089 ( $\nu_a S=O$ , sulfonate group of PyrZIC) → 1175 (in-plane C—H, pyrrolidium ring of PyrZIC) → 1196 (in-plane C—H, pyrrolidium ring of PyrZIC) → 1318 ( $\nu_a S=O$ , TFSI anion of LiTFSI) → 1064 ( $\nu_a S=O$ , sulfonate group of PyrZIC) → 1125 (twisting C—H, pyrrolidium ring of PyrZIC) → 1336 (in-phase  $\nu_s S=O$ , TFSI anion of LiTFSI)  $\text{cm}^{-1}$  in region II. Region I includes three kinds of pyrrolidinium rings (1151, 1134, and 1122  $\text{cm}^{-1}$  for twisting C—H) and two kinds of sulfonate group (1064 and 1050  $\text{cm}^{-1}$  for  $\nu_a S=O$ ), while region II has four kinds of pyrrolidinium rings (1196 and 1175  $\text{cm}^{-1}$  for in-plane C—H and 1156 and 1125  $\text{cm}^{-1}$  for twisting C—H) and two kinds of sulfonate groups (1089 and 1064  $\text{cm}^{-1}$  for  $\nu_a S=O$ ). Regions I and II show the additional peaks split by an asynchronous 2D correlation spectra, which were not readily detectable in the 1D spectra. Therefore, these findings indicate that the characteristic peaks of binary ionic gels were split due to the interactions among functional groups and the respective dynamic behaviors in regions I and II were attributed to the unique conformational changes under the different chemical environments.

## CONCLUSION

In this research, binary ionic gels were synthesized by simply mixing two ionic salts, PyrZIC and LiTFSI. The binary ionic gels showed thermal transitions and physical gelation with respect to the chemical compositions of ionic salts as analyzed by TGA and DSC. The transition behaviors of binary ionic gels were attributed to the formation of binary IL-like domains by means of the specific interactions between the pyrrolidinium rings of PyrZICs and TFSI anions of LiTFSIs. The dynamics of transition and the interactions were characterized by DFT, PCA, and 2D IR COS. The interactions between PyrZICs and LiTFSIs at the molecular level were theoretically analyzed by DFT. The optimized geometries of PyrZIC interacting with LiTFSI were calculated by DFT, showing energetic stabilization via hydrogen bonding between hydrogen atoms of PyrZIC and oxygen atoms of the TFSI group and electrostatic interactions between lithium cations of LiTFSI and oxygen atoms of PyrZIC. The intermolecular interactions of binary ionic gels were accompanied by conformational changes, and their chemical compositions led to different dynamic processes in regions I and II, which were divided by the transition point of PCA plots. 2D IR COS was used to analyze the respective dynamic behaviors of regions I and II. In particular, region II revealed the characteristic pattern of a four-leaf-clover cluster for the synchronous 2D correlation spectrum and the butterfly pattern for the asynchronous 2D correlation spectrum due to the conformational changes under the unique chemical

circumstances different from those of region I. Furthermore, the respective kinetics of conformational changes in regions I and II demonstrated different sequences of changes in spectral intensities. Therefore, the thermal transitions and physical gelation of binary ionic gels are strongly influenced by conformational changes in the interaction fields according to chemical compositions.

## ASSOCIATED CONTENT

**S Supporting Information.** XRD patterns, UV-vis spectra, and DFT results. This material is available free of charge via the Internet at <http://pubs.acs.org>.

## AUTHOR INFORMATION

### Corresponding Author

\*Phone: +82 31 201 3327. E-mail: phs0727@khu.ac.kr (H.S.P.); ymjung@kangwon.ac.kr (Y.M.J.).

## ACKNOWLEDGMENT

This work was supported by the GRRC program of Gyeonggi province [GRRC Kyung Hee 2010-B04] and grants (AC3-101) from Carbon Dioxide Reduction and Sequestration Research Center, one of the 21st Century Frontier Programs funded by the Ministry of Science and Technology of Korean government and Kolon Industries Co.

## REFERENCES

- (1) (a) Hirst, A. R.; Escuder, B.; Miravet, J. F.; Smith, D. K. *Angew. Chem., Int. Ed.* **2008**, *47*, 8002–8018. (b) Nayak, S.; Lyon, L. A. *Angew. Chem., Int. Ed.* **2005**, *44*, 7686–7708. (c) Sangeetha, N. M.; Maitra, U. *Chem. Soc. Rev.* **2005**, *34*, 821–836. (d) Banerjee, S.; Das, R. K.; Maitra, U. *J. Mater. Chem.* **2009**, *19*, 6649–6687.
- (2) (a) Gadjourova, Z.; Andreev, Y. G.; Tunstall, D. P.; Bruce, P. G. *Nature* **2001**, *412*, 520–523. (b) Zhang, C.; Andreev, Y. G.; Bruce, P. G. *Angew. Chem., Int. Ed.* **2007**, *46*, 2848–2850. (c) Abu-Lebdeh, Y.; Alarco, P.-J.; Armand, M. *Angew. Chem., Int. Ed.* **2003**, *42*, 4499–4501. (d) MacFarlane, D. R.; Forsyth, M. *Adv. Mater.* **2001**, *13*, 957–966.
- (3) (a) Yoshizawa, M.; Hirao, M.; Ito-Akita, K.; Ohno, H. *J. Mater. Chem.* **2001**, *11*, 1057–1062. (b) Tiyapiboonchaiya, C.; Pringle, J. M.; Sun, J.; Byrne, N.; Howlett, P. C.; MacFarlane, D. R.; Forsyth, M. *Nat. Mater.* **2004**, *3*, 29–32. (c) Nguyen, D. Q.; Hwang, J.; Lee, J. S.; Kim, H.; Lee, H.; Cheong, M.; Lee, B.; Kim, H. S. *Electrochim. Commun.* **2007**, *9*, 109–114. (d) Narita, A.; Shibayama, W.; Ohno, H. *J. Mater. Chem.* **2006**, *16*, 1475–1482. (e) Kim, H. S.; Bae, J. Y.; Park, S. J.; Lee, H.; Bae, H. W.; Kang, S. O.; Lee, S. D.; Choi, D. K. *Chem.—Eur. J.* **2007**, *13*, 2655–2660. (f) Lee, H.; Kim, D. B.; Kim, S. H.; Kim, H. S.; Kim, S. J.; Choi, D. K.; Kang, Y. S.; Won, J. *Angew. Chem., Int. Ed.* **2004**, *43*, 3053–3056.
- (4) Park, H. S.; Kwon, S. R.; Jung, Y. M.; Kim, H. S.; Lee, H. J.; Hong, W. H. *Chem. Commun.* **2009**, 6388–6390.
- (5) (a) Byrne, N.; Howlett, P. C.; MacFarlane, D. R.; Forsyth, M. *Adv. Mater.* **2005**, *17*, 2497–2501. (b) Narita, A.; Shibayama, W.; Sakamoto, K.; Mizumo, T.; Matsumi, N.; Ohno, H. *Chem. Commun.* **2006**, 1926–1928.
- (6) (a) Sun, J.; MacFarlane, D. R.; Byrne, N.; Forsyth, M. *Electrochim. Acta* **2006**, *51*, 4033–4038. (b) Byrne, N.; MacFarlane, D. R.; Forsyth, M. *Electrochim. Acta* **2005**, *50*, 3917–3921.
- (7) (a) Yoshizawa, M.; Xu, W.; Angell, C. A. *J. Am. Chem. Soc.* **2003**, *125*, 15411–15419. (b) Noda, A.; Susan, Md. A. B. H.; Kudo, K.; Mitsushima, S.; Hayamizu, K.; Watanabe, M. *J. Phys. Chem. B* **2003**, *107*, 4024–4033. (c) Yoshizawa, M.; Ogihara, W.; Ohnoz, H. *Electrochim. Solid State Lett.* **2001**, *4*, E25–E27.
- (8) (a) Köddermann, T.; Wertz, C.; Heintz, A.; Ludwig, R. *Angew. Chem., Int. Ed.* **2006**, *45*, 3697–3702. (b) Rivera-Rubero, S.; Baldelli, S.

*J. Am. Chem. Soc.* **2004**, *126*, 11788–11789. (c) Zhao, Y.; Gao, S.; Wang, J.; Tang, J. *J. Phys. Chem. B* **2008**, *112*, 2031–2039. (d) Mele, A.; Tran, C. D.; Lacerda, S. H. D. *Angew. Chem., Int. Ed.* **2003**, *42*, 4364–4366.

(9) Rivera-Rubero, S.; Baldelli, S. *J. Am. Chem. Soc.* **2004**, *126*, 11788–11789.

(10) Vadejinste, B. G. M.; Massart, D. L.; Buydens, L. M. C.; DeJong, S.; Lewi, P. J.; Smeyers-Verbeke, J. *Handbook of Chemometrics and Qualimetrics: Part B*; Elsevier Science B. V.: Amsterdam, The Netherlands, 1998, p 88.

(11) Ozaki, Y.; Noda, I. *Two-Dimensional Correlation Spectroscopy: Applications in Vibrational Spectroscopy*; John Wiley & Sons, Inc.: New York, 2004. Noda, I. *Appl. Spectrosc.* **1993**, *47*, 1329–1336.

(12) (a) Umebayashi, Y.; Mitsuji, T.; Fukuda, S.; Fujimori, T.; Fujii, K.; Kanzaki, R.; Takeuchi, M.; Ishiguro, S.-I. *J. Phys. Chem. B* **2007**, *111*, 13028–13032. (b) Hayashi, S.; Ozawa, R.; Hamaguchi, H. *Chem. Lett.* **2003**, *32*, 498–499. (c) Saha, S.; Hayashi, S.; Kobayashi, A.; Hamaguchi, H. *Chem. Lett.* **2003**, *32*, 740–741. (d) Ozawa, R.; Hayashi, S.; Saha, S.; Kobayashi, A.; Hamaguchi, H. *Chem. Lett.* **2003**, *32*, 948–949.

(13) Izgorodina, E. I.; Bernard, U. L.; MacFarlane, D. R. *J. Phys. Chem. A* **2009**, *113*, 7064–7072.

(14) Becke, A. D. *J. Chem. Phys.* **1993**, *98*, 5648–5652.

(15) (a) Lean, A. D.; Chandler, G. S. *J. Chem. Phys.* **1980**, *72*, 5639–5648. (b) Ditchfield, R.; Hehre, W. J.; Pople, J. A. *J. Chem. Phys.* **1971**, *54*, 724–728. (c) Frisch, M. J.; Pople, J. A.; Binkley, J. S. *J. Chem. Phys.* **1984**, *80*, 3265–3269.

(16) (a) Jung, Y. M.; Noda, I. *Appl. Spectrosc. Rev.* **2006**, *41*, 515–547.

(b) Noda, I. *Appl. Spectrosc.* **1993**, *47*, 1329–1336.

(17) (a) Park, H. S.; Choi, Y. S.; Jung, Y. M.; Hong, W. H. *J. Am. Chem. Soc.* **2008**, *130*, 845–852. (b) Park, H. S.; Jung, Y. M.; You, J. K.; Hong, W. H.; Kim, J. N. *J. Phys. Chem. A* **2008**, *112*, 6558–6562.

(18) Liang, H.; Li, H.; Wang, Z.; Wu, F.; Chen, L.; Huang, X. *J. Phys. Chem. B* **2001**, *105*, 9966–9969.

(19) (a) Yoshizawa, M.; Hirao, M.; Ito-Akita, K.; Ohno, H. *J. Mater. Chem.* **2001**, *11*, 1057–1062. (b) Narita, A.; Shibayama, W.; Ohno, H. *J. Mater. Chem.* **2006**, *16*, 1475–1482.

(20) (a) Yoshizawa, M.; Ohno, H. *Chem. Commun.* **2004**, 1828–1829. (b) Ohno, H.; Yoshizawa, M.; Ogihara, W. *Electrochim. Acta* **2003**, *48*, 2079–2083.